Post-print of: Mazierski P., Łuczak J., Lisowski W., Winiarski M., Klimczuk T., Zaleska-Medynska A.: The ILs-assisted electrochemical synthesis of TiO2 nanotubes: The effect of ionic liquids on morphology and photoactivity. APPLIED CATALYSIS B-ENVIRONMENTAL. Vol. 214, (2017), p. 100-113. DOI: 10.1016/j.apcatb.2017.05.005

The ILs-assisted electrochemical synthesis of TiO_2 nanotubes: The effect of ionic liquids on morphology and photoactivity

P. Mazierski [a], J. Łuczak [b], W. Lisowski [c], M.J. Winiarski [d], T. Klimczuk [d], A. Zaleska-Medynska [a]

[a] Department of Environmental Technology, Faculty of Chemistry, University of Gdansk, Wita Stwosza 63, 80-308 Gdansk, Poland
[b] Department of Chemical Technology, Faculty of Chemistry, Gdansk University of Technology, G. Narutowicza 11/12, 80-233 Gdansk, Poland
[c] Mazovia Center for Surface Analysis, Institute of Physical Chemistry, Polish Academy of Science, Kasprzaka 44/52, 01-244 Warszawa, Poland
[d] Department of Solid State Physics, Faculty of Applied Physics and Mathematics, Gdansk University of Technology, 80-233 Gdansk, Poland

a b s t r a c t

Facile and environmentally benign one-step titanium anodization method for TiO_2 nanotubes (NTs) for-mation in a presence of ionic liquids (ILs) was proposed. Influence of the IL structure and its content in ethylene glycol electrolyte on morphology, surface properties and photoactivity of the TiO_2 NTs was investigated. Possible interactions between IL and TiO_2 NTs as well as the mechanism of NTs formation during anodic oxidation process were proposed. The outer diameter, wall thickness, and length of the IL-NTs were found to be proportionally related with increasing length of the hydrocarbon chain in the imidazolium cation of the IL (from 2 to 8), IL content, anodization potential and water content up to 10 vol.%. Moreover, for the first time, the effect of the IL's structure on the UV–vis and Vis light-induced photoactivity of the IL-TiO_2 NTs was presented, and the active species ($^{\bullet}OH$ and $O_2^{\bullet-}$ radicals) involved in the photocatalytic reaction of phenol degradation were determined. The sample that exhibited the highest photoactivity under Vis irradiation (0.63 μmol dm^{-3} min^{-1}) and greatest amounts of generated

$^{\bullet}OH$ was TiO_2 NTs prepared at anodization potential 90 V in the electrolyte containing 0.1 mol of 1-octyl-3-methylimidazolium tetrafluoroborate [OMIM][BF_4] (represented by F^- content) and 10 vol.% of water. Phenol degradation rate remained at level about 1.50 and 0.42 μmol dm^{-3} min^{-1} after 60 min of UV–vis and Vis irradiation after four cycles in the presence of [OMIM][BF_4] and thus obtained IL-NTs exhibited photostability. The reaction proceeds under mild reaction conditions, is step economical and provides one-dimensional nanostructures that meet the specifications for use in diverse photocatalytic applications.

Keywords: TiO_2 nanotubes, Ionic liquid, Electrochemical method, Phenol degradation Visible, light photoactivity, Nitrogen and boron doping

1. Introduction

Over the past several dozen years, many photocatalytic applications, using titanium dioxide (TiO_2) as photocatalyst, have been proposed. Self-cleaning surfaces, air and water purification, dye-sensitized solar cells, sterilization as well as water splitting to hydrogen [1,2] belong to the most important. Among versatile morphologies of TiO_2 the hierarchical, oriented 1D semiconductor nanostructures nanotubes (NTs) are receiving particular attention due to their unusual properties rather than bulk [3–6]. Especially electronic properties including high electron mobility or quantum confinement effects, low dimensionality as well as high surface to volume ratio are of great interest since provides increased activity/reactivity of TiO_2 [7].

In recent years' ionic liquids (ILs) emerged as important reaction environment or structuring agent for nano- and microstructures preparation [8–11]. The great interest in application of the ILs in this area is based on their unique and highly customizable properties such as negligible volatility, high polarity, non-flammability, wide liquid range, good dissolving properties as well as microwave absorbing ability etc [8]. Ionic liquids can work as a reaction environment [12,13], co-solvent or structuring agents [14–16] due to their ability to form protective layers, by steric, electrostatic, viscous protection or solvation forces stabilizing growing colloidal structures as well as being able to create a soft template for nanostructures (micelles or microemulsions) [17–21]. Many versatile synthesis methods were up to date applied for preparation of TiO_2

http://dx.doi.org/10.1016/j.apcatb.2017.05.005

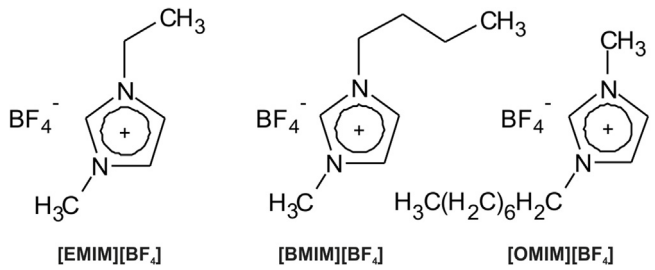

Fig. 1. Structure of 1-ethyl-3-methylimidazolium tetrafluoroborate [EMIM][BF_4], 1-butyl-3-methylimidazolium tetrafluoroborate [BMIM][BF_4] and 3-methyl-1-octylimidazolium tetrafluoroborate [OMIM][BF_4] ionic liquids used for NTs formation.

with different morphologies, however much less studies were performed in the field of the IL-assisted synthesis of the nano- and microstructures using electrochemical methods [9]. However, ILs as electrochemically stable, non-volatile and highly conducting solvents seems to be excellent media to directly anodize titanium or play a role of F^- anions source generated *in situ* providing TiO_2 NTs with low-defects. Ionic liquids reveal a low IR drop during anodization process, therefore results in slow decomposition [22]. In contrast to the other methods, the electrochemical anodization approach provides dense and well-defined layer, where NTs are perpendicularly aligned to the substrate surface. Moreover, growth of the well-defined NTs with controllable length is achieved in very short time [23].

One of the first work revealing feasibility of using 1-butyl-3-methylimidazolium tetrafluoroborate [BMIM][BF_4] as solvent for NTs preparation was published by Schmuki group [24], who prepared NTs using relatively low anodization potentials (5–10 V). Continuing these studies, Dai group improves anodization conditions in [BMIM][BF_4] obtaining much longer and wider nanostructures (length exceeded 4 μm) [22,25]. Water content was also found to be a crucial parameter for formation of well-aligned long NTs, especially for the higher anodization potentials with optimum content at 2.4 wt% [25]. The same IL, however, used as structuring agent, was applied by Misra et al. for the double-walled TiO_2 NTs formation using the sonoelectrochemical process at the anodization potential above 60 V. Such structures (with diameter even above 200 nm) were found to have 2–6 times higher photocurrent density in the reaction of water photooxidation under solar light illumination when compared to the conventional NTs and commercial TiO_2 nanoparticles [26]. Titania NTs were also tested for the photodegradation of methyl orange dye as well as hydrogen evolution from water/methanol solutions by UV irradiation [27]. Summarizing, one of the challenges in this area of research is development of the effective route to synthesize desired nanostructures with uniformity in size and distribution, controlled morphology without defects and consequently desired and improved properties. Nevertheless, as shown above data on the role of the IL's structure in the mechanism of the TiO_2 NTs formation and in the mechanism of ILs-modified TiO_2 excitation is still limited. The effect of the IL structure on the ability to interact with TiO_2 surface, and therefore on the TiO_2 properties has not been yet described, and therefore is not clear.

Considering the points in the above discussion, in this paper we present the effect of the IL structure (the alkyl chain length in the cation) as well as amount of IL (thus fluoride) and water content used during synthesis on the morphology, surface properties and photoactivity of TiO_2 NTs. However, due to the relatively high price of ILs, we propose using IL as structuring agent for formation of NTs with controllable length and desired properties. Therefore, three ionic liquids containing easily hydrolysable [BF_4] anion and different chain length in the imidazolium cation, shown in Fig. 1, were chosen. For the first time morphology and surface properties of TiO_2 NTs prepared in the presence of structurally differentiated ILs were correlated with their photocatalytic performance as well as ability to form hydroxyl radical, based on detection of fluorescent product of terephthalic acid hydroxylation. The role of the ionic liquids in the TiO_2 NTs preparation, stabilization and photoactivity enhancement was proposed.

2. Experimental

2.1. Materials

Ionic liquids 1-ethyl-3-methylimidazolium tetrafluoroborate [EMIM][BF_4], 1-butyl-3-methylimidazolium tetrafluoroborate [BMIM][BF_4], and 3-methyl-1-octylimidazolium tetrafluoroborate [OMIM][BF_4] with purity of ≥99%, were purchased from Iolitec, Germany. Ionic liquids were degassed and dried under vacuum before use (Thermo VT6025, Germany) for at least 24 h at 80 °C. The water content in these ILs were determined by coulometric Karl-Fischer titration method (Coulometer model 899, Metrohm) and was less than 700 ppm. Titania NT arrays were obtained by anodization of Ti foil (0.127 mm thickness, 99.7% purity, Sigma-Aldrich). Isopropanol (p.a., POCh S.A., Poland), acetone, methanol (p.a., P.P.H. STANLAB, Poland) and deionized water (Hydrolab BASIC 5, Poland) were used for cleaning Ti substrate surface. The Ti substrate was anodized in solutions composed of ethylene glycol (EG, 99.0%, p.a., POCh S.A. Poland), deionized water and selected IL. Phenol (99.5%, p.a., POCh S.A., Poland) as well as terephthalic acid (98%, p.a., Sigma-Aldrich) were used as model compounds for the photoactivity characterization.

2.2. Physicochemical characteristics of electrolytes

Dynamic viscosity of the electrolytes containing ILs used for NTs preparation were measured using cone-plate viscometer LVDV-III, Brookfield Engineering Laboratory, USA. Density measurements were carried out by oscillation method using DM40 LiquiPhysics™ Excellence density meter, Mettler Toledo, USA. Conductivity measurements were performed using a CX-701 conductivity meter, Elmetron, Poland. Surface tension of the solutions was determined using goniometric technique in the pendant drop mode, with a video based optical contact angle meter OCA 15, Dataphysics, Germany. The temperature of all measurements was maintained at a constant level of 25 ± 0.1 °C with a thermostatic baths PolyScience AD07R-20, USA (viscosity, conductivity, surface tension) or by a Peltier-type electronic temperature controller provided by the apparatus (density).

2.3. Preparation of the IL-assisted TiO_2 NTs

Prior to use, Ti foil was cleaned by sonication in acetone, isopropanol, methanol and deionized water for 10 min in each solvent and dried in air stream. The anodic oxidation was carried out in a three-electrode electrochemical set-up, where Ti foil (3 × 2 cm) was used as a working electrode, a Pt mesh as a counter electrode and a Ag/AgCl reference electrode for process controll and to obtain information about actual working electrode potential. Anodization was performed in the electrolyte composed of ethylene glycol, deionized water and selected IL for 20 min at the voltage range of 60–90 V, using programmable DC power supply (MCP M10-QS1005). For measurement of actual current and potential of Ti electrode versus Ag/AgCl reference electrode digital multimeter (BRYMEN BM857a) was applied. As prepared titania NTs were rinsed with deionized water followed by sonication also in deionized water (5 min), drying in air at 80 °C (24 h) and calcination at 450 °C (heating rate 2 °C/min).

Table 1
Physicochemical properties of the electrolytes and pure ILs used for NTs preparation.

	Sample label	Electrolyte composition	Dynamic viscosity [mPa s]	Density [kg dm^{-1}]	Conductivity (S m^{-1})	Surface tension [mN m^{-1}]
Pure ILs	[EMIM][BF_4]	–	38.45 ± 0.66	1.2813 ± 0.0001	38.45 ± 0.66	50.87 ± 0.11
	[BMIM][BF_4]	–	108.5 ± 0.34	1.2016 ± 0.0002	108.5 ± 0.34	44.92 ± 0.15
	[OMIM][BF_4]	–	332.2 ± 0.99	1.1035 ± 0.0001	332.2 ± 0.99	32.93 ± 0.21
ILs-based electrolytes	[EMIM][BF_4]	EG, 10 vol.% H_2O, 0.1 mol F^- from [EMIM][BF_4]	11.58 ± 0.07	1.1039 ± 0.0001	216.70 ± 0.17	49.56 ± 0.24
	[BMIM][BF_4]	EG, 10 vol.% H_2O, 0.1 mol F^- from [BMIM][BF_4]	11.62 ± 0.02	1.1037 ± 0.0001	201.64 ± 1.11	49.12 ± 0.04
	[OMIM][BF_4]	EG, 10 vol.% H_2O, 0.1 mol F^- from [OMIM][BF_4]	11.66 ± 0.05	1.1032 ± 0.0001	168.82 ± 0.54	48.38 ± 0.14
	0.2 mol F^-	EG, 10 vol.% H_2O, 0.2 mol F^- from [OMIM][BF_4]	11.72 ± 0.07	1.1031 ± 0.0001	299.23 ± 1.41	47.67 ± 0.03
	0.3 mol F^-	EG, 10 vol.% H_2O, 0.3 mol F^- from [OMIM][BF_4]	11.84 ± 0.09	1.1031 ± 0.0001	415.30 ± 1.30	46.01 ± 0.09
	0% H_2O	EG, 0 vol.% H_2O, 0.1 mol F^- from [OMIM][BF_4]	16.37 ± 0.02	1.1095 ± 0.0001	114.11 ± 2.34	47.08 ± 0.07
	2.5% H_2O	EG, 2.5 vol.% H_2O, 0.1 mol F^- from [OMIM][BF_4]	15.00 ± 0.05	1.1079 ± 0.0001	129.12 ± 1.33	47.42 ± 0.02
	5% H_2O	EG, 5 vol.% H_2O, 0.1 mol F^- from [OMIM][BF_4]	13.91 ± 0.08	1.1066 ± 0.0001	147.24 ± 3.92	47.45 ± 0.05
	15%H_2O	EG, 15 vol.% H_2O, 0.1 mol F^- from [OMIM][BF_4]	9.88 ± 0.09	1.0995 ± 0.0001	189.59 ± 1.37	49.09 ± 0.24

The IL concentration in the electrolyte before and after anodization was determined by high performance liquid chromatography (HPLC, Shimadzu). The HPLC system was equipped with a Kinetex C18 column (150 mm × 3 mm; particle size of 2.6 μm; pore diameter 100 Å). The flow rate was maintained at 0.4 mL/min with a mobile phase composed of acetonitrile and water (v/v: 50/50), and the SPD-M20A diode array detector was operated at 200 nm.

2.4. Surface properties characterization

The morphology of the TiO_2 NTs in the form of a thin film was determined by scanning electron microscopy (SEM, FEI Quanta 250 FEG). NT lengths were measured using a tilted (30°) sample holder. The results given in the text are corrected for the effect of tilt. X-ray photoelectron spectroscopy (XPS) experiments were performed using a PHI 5000 VersaProbeTM (ULVAC-PHI) spectrometer with monochromatic Al Kα radiation ($h\nu$ = 1486.6 eV). The X-ray beam was focused to a diameter of 100 μm, and the measured area was defined as a 250 μm square. The high-resolution (HR) XPS spectra were collected by the hemispherical analyzer at pass energy of 23.5 eV, an energy step size of 0.1 eV and a photoelectron take off angle of 45° with respect to the surface plane. CasaXPS software was used to evaluate the XPS data. The HR XPS spectra were deconvoluted using a Shirley background and a Gaussian peak shape with 30% Lorentzian character. The binding energy (BE) scale of all detected spectra was referenced by setting the BE of the aliphatic carbon peak (C—C) signal to 284.6 eV. The X-ray diffraction (XRD) measurements were conducted on PhillipsX'Pert Pro MPD diffractometer with CuKα radiation. The XRD patterns were processed by means of LeBail refinement using FULLPROF 5.30 software [28].

2.5. Measurement of photocatalytic activity

The photocatalytic properties of the obtained NTs were determined by a two-model process: treatment of water from phenol and •OH radical generation efficiency (using terephthalic acid) under both UV and Vis light irradiation as it was described in our previous papers [29–31]. Minor changes were as follows: photocatalytic activity tests in the water phase (phenol degradation and •OH radical generation) were carried out in a photoreactor made of quartz with a working volume of approximately 10 mL. The phenol and terephthalic acid concentration was 0.21 mM and 0.5 mM, respectively. The photocatalysts with the surface area of 4 cm^2 were immersed in phenol or terephthalic acid solution for 30 min in the dark to achieve the adsorption-desorption equilibrium. Subsequently, the reaction system was irradiated with a 1000 W Xenon lamp (Oriel 66021) under magnetic stirring (500 rpm). For the visible-light tests activity, the light beam was passed through GG420 filter to cut-off wavelengths shorter than 420 nm. Reference phenol and terephthalic acid samples (0.5 mL) were taken just before starting the irradiation, and subsequent samples (0.5 mL) were collected at regular time periods (20 min) during irradiation. Phenol concentration was estimated by the colorimetric method after derivatization with *p*-nitroaniline using UV–vis spectrophotometer (λ = 480 nm). Fluorescence spectra were recorded at room temperature by using a LS–50 B Luminescence Spectrophotometer equipped with Xenon discharge lamp as an excitation source (excitation wavelength 315 nm) and a R928 photomultiplier detector. Irradiation intensity was measured by an optical power meter (HAMAMATSU, C9536-01) and equaled 30 and 4 mW/cm^2 for UV–vis and Vis irradiation, respectively. The distance between the photoreactor and the lamp reached 30 cm^2. Kinetics of phenol degradation by-products have been followed by high performance liquid chromatography (HPLC, Shimadzu). The flow rate was maintained at 0.4 mL/min with a mobile phase composed of acetonitrile and water (v/v: 7.5/92.5), with a sample injection volume of 30 μL, and the SPD-M20A diode array detector was operated at 205 nm.

3. Results and discussion

3.1. Physicochemical characteristics of electrolytes

Since formation of the NTs in viscous electrolytes yields 1D structures with smooth tube walls [32], addition of the IL may be useful due to possibility to adjust viscosity of the electrolyte. The electrolyte compositions has been carefully chosen to examine: (i) the effect of the ILs' cation (the amount of the ILs in electrolyte was chosen to keep the same content of fluoride ions (0.1 mol F^-), (ii) the influence of F^- content (0.1, 0.2 or 0.3 mol F^-), and (iii) the effect of amount of water (0–15 vol.% H_2O).

It was observed that physicochemical properties of the electrolytes composed of different ILs (0.1 mol F^-), water (10 vol%) and ethylene glycol are not determined solely by the properties of the ILs but also the other components (Table 1). As expected applica-

tion of the IL with longer alkyl substituent in the imidazolium cation resulted in increase of the dynamic viscosity of the IL-bearing electrolytes, and values from 11.58 to 11.66 mPa s were detected. The viscosity rise in a systematic manner can be related with increase of the effect of the Van der Waals interactions that predominate electrostatic ones as the side-chain length in IL increases [33]. The same reason may result in decrease of density, electrical conductivity and surface tension of electrolytes with increasing length of the alkyl chain on the imidazolium cation added. Such trends are well documented in the literature for pure ILs [34]. Addition up to 15 vol.% of water to the EG/[OMIM][BF_4] system resulted in decrease of the electrolyte dynamic viscosity (from 16.37 to 9.88 mPa s) and density (from 1.1095 to 1.0995 g cm^{-3}) accompanied by the increase in the specific conductivity (from 114.11 to 189.59 S m^{-1}) and surface tension (from 47.08 to 49.09 mN m^{-1}). These relations, being dependent predominantly on differences in properties of pure glycol and water, are in agreemen with available literature for EG/water mixtures [35]. Increasing content of F^-, reflected by amount of the IL in the electrolyte, resulted in increase of the dynamic viscosity (from 11.66 to 11.84 mPa s) and conductivity (from 168.82 to 415.30 S m^{-1}) due to significantly higher values of this parameters characteristic for ILs in comparison to the other components of the system. Additionally, surface tension of the electrolytes decreased from 48.38 to 46.01 mN m^{-1} as detected for 0.1 and 0.3 mol F^-, whereas changes of density were insignificant.

3.2. Morphology and crystal structure

Application of the selected ILs enables formation of NTs with uniform length, diameter and smooth walls with low microstructural defects. To remove the porous layer formed on the top surface of the NTs, the ultrasonic treatment in water just after anodization was applied. As evident from the observations of SEM images presented in Figs. 2–5 ultrasonically treated NTs were free of surface contamination, were open, thus easily accessible to light irradiation and reagents in the photocatalytic reaction. The sample labels of as-prepared NTs together with composition of electrolytes used for preparation, and selected features of NTs are presented in Table 2.

3.2.1. Effect of the ionic liquid's cation structure

Obtaining results revealed that anodization of the Ti substrate in the electrolyte containing the IL with longer alkyl substituent in the imidazolium cation provides longer NTs with larger outer and inner diameter, as presented in Fig. 2. In this regard, TiO_2 NTs with length of 0.35 μm and outer diameter 100 nm were obtained for the reaction system containing [EMIM][BF_4] (NTs_[EMIM] sample), whereas these parameters increased to 0.7 μm and 120 nm, respectively for NTs_[OMIM] sample.

3.2.2. Effect of the anodization potential

To assess the effect of the anodization potential on the NT dimension and morphology, a series of samples using potential from 60 V to 90 V and the IL that provided the NTs with the highest dimensions were chosen. The [OMIM][BF_4] content represented by F^- concentration and amount of water were constant and equal to 0.1 mol F- and 10 vol.%, respectively. The outer diameter, wall thickness, and length of the IL-NTs were found to be proportionally related with increasing anodization potential. The length of the IL-NTs prepared at 60 V was 0.2 μm (NTs_[OMIM]_60V) and increased to 0.85 μm for 90 V (NTs_[OMIM]_90V). At the same time, the outer diameter changed from 90 up to 135 nm, respectively (see Fig. 3). Furthermore, the top view for the NTs prepared at 60 V presented typical initiation layer (the early stage of anodization) and suggested that too weak anodization conditions were used.

Table 2
Sample labels, characterization and photocatalytic activity of IL-TiO_2 NTs.

Sample label	EG/ILs-based electrolyte composition used for NTs preparation and anodization parameters	Crystallite size (nm)	Cell parameters (A)		Cell volume, V (A^3)	NTs length (μm)	Photocatalytic degradation rate of phenol, r (μmol dm^3 min^{-1})	
			a = b	c			UV–vis (λ > 350 nm)	Vis (λ > 420 nm)
NTs_[EMIM]	EG, 10 vol.% H_2O, 0.1 mol F^- from [EMIM][BF_4], 80 V, 20 min	33	3.8077(7)	9.741(1)	141.23(7)	0.35	1.00	0.20
NTs_[BMIM]	EG, 10 vol.% H_2O, 0.1 mol F^- from [BMIM][BF_4], 80 V, 20 min	39	3.8005(6)	9.735(1)	140.61(6)	0.45	1.26	0.30
NTs_[OMIM]	EG, 10 vol.% H_2O, 0.1 mol F^- from [OMIM][BF_4], 80 V, 20 min	31	3.8036(7)	9.740(1)	140.91(7)	0.70	1.53	0.48
NTs_[OMIM]_60V	EG, 10 vol.% H_2O, 0.1 mol F^- from [OMIM][BF_4], 60 V, 20 min	31	3.8024(8)	9.735(1)	140.76(7)	0.20	0.45	0.16
NTs_[OMIM]_70V	EG, 10 vol.% H_2O, 0.1 mol F^- from [OMIM][BF_4], 70 V, 20 min	39	3.8040(6)	9.739(1)	140.93(6)	0.60	1.31	0.41
NTs_[OMIM]_90V	EG, 10 vol.% H_2O, 0.1 mol F^- from [OMIM][BF_4], 90 V, 20 min	36	3.8027(5)	9.739(1)	140.83(5)	0.85	1.82	0.63
NTs_[OMIM]_0.2F^-	EG, 10 vol.% H_2O, 0.2 mol F^- from [OMIM][BF_4], 80 V, 20 min	50	3.8039(5)	9.739(7)	140.92(14)	0.75	1.58	0.53
NTs_[OMIM]_0.3F^-	EG, 10 vol.% H_2O, 0.3 mol F^- from [OMIM][BF_4], 80 V, 20 min	38	3.8032(6)	9.739(1)	140.87(6)	0.81	1.65	0.55
NTs_[OMIM]_0%H_2O	EG, 0 vol.% H_2O, 0.1 mol F^- from [OMIM][BF_4], 80 V, 20 min	22	3.8135(9)	9.737(2)	141.60(10)	0.20	0.63	0.25
NTs_[OMIM]_2.5%H_2O	EG, 2.5 vol.% H_2O, 0.1 mol F^- from [OMIM][BF_4], 80 V, 20 min	33	3.8071(7)	9.741(1)	141.19(7)	0.30	0.76	0.32
NTs_[OMIM]_5.0%H_2O	EG, 5 vol.% H_2O, 0.1 mol F^- from [OMIM][BF_4], 80 V, 20 min	34	3.8034(6)	9.741(1)	140.91(6)	0.65	1.40	0.39
NTs_[OMIM]_15%H_2O	EG, 5 vol.% H_2O, 0.1 mol F^- from [OMIM][BF_4], 80 V, 20 min	47	3.8001(5)	9.734(9)	140.57(17)	0.35	0.89	0.36

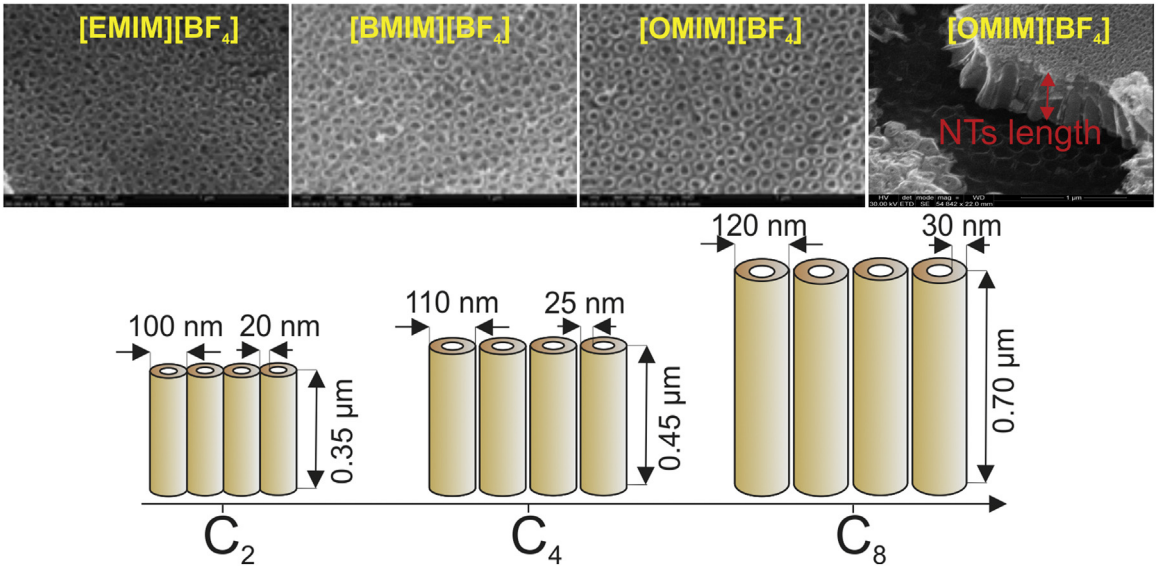

Fig. 2. Effect of the IL's cation on the morphology of TiO_2 NTs. Fluoride content 0.1 mol, water content 10 vol%, anodization potential 80 V.

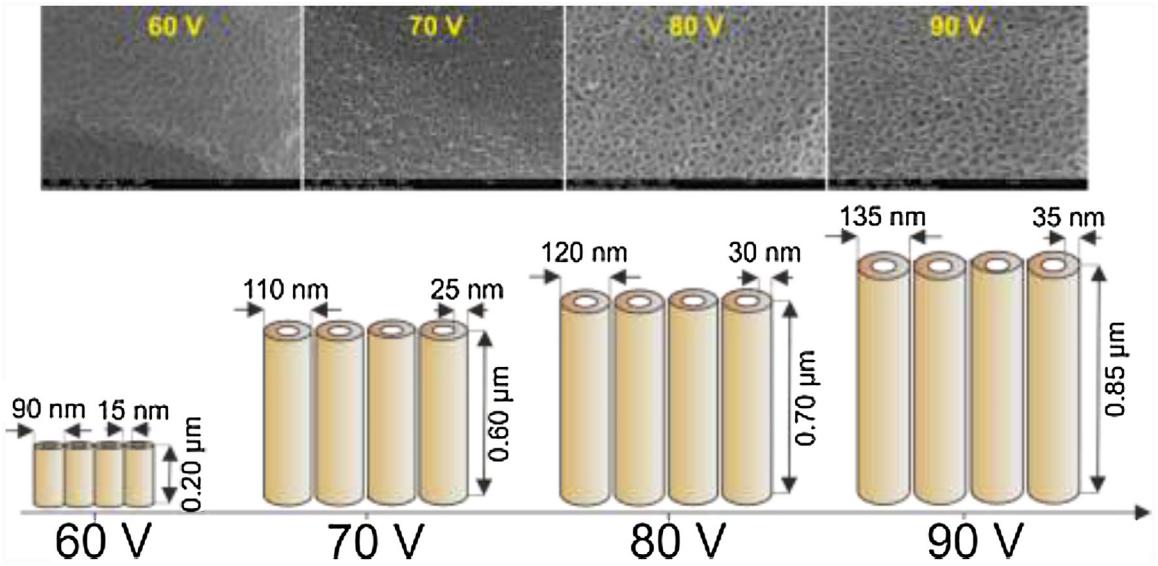

Fig. 3. Effect of the anodization potential on the morphology of TiO_2 NTs prepared in the presence of EG/[OMIM][BF_4]-based electrolyte. Fluoride content 0.1 mol, water content 10 vol.%.

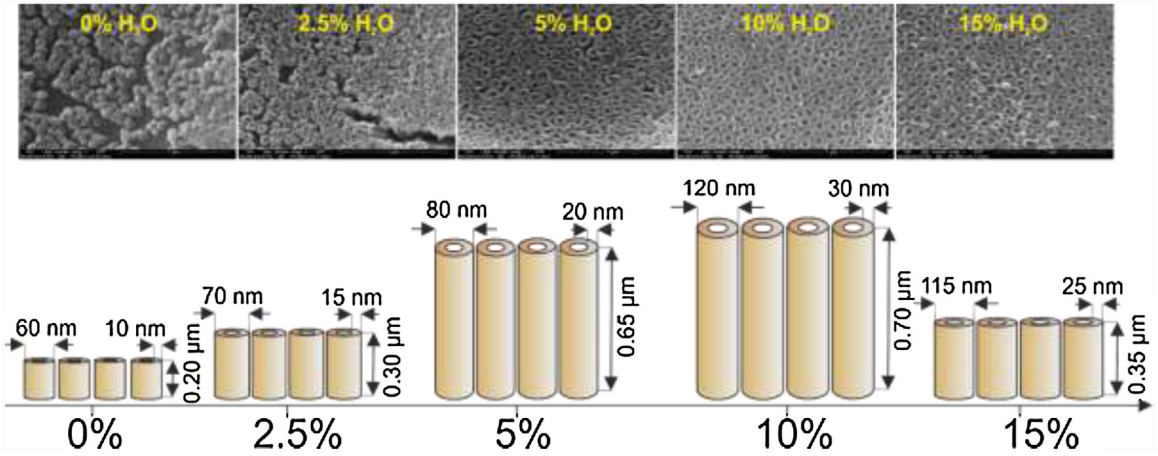

Fig. 4. Effect of the water content on the morphology of the TiO_2 NTs prepared in the presence of EG/[OMIM][BF_4]-based electrolyte. Fluoride content 0.1 mol, anodization potential 80 V.

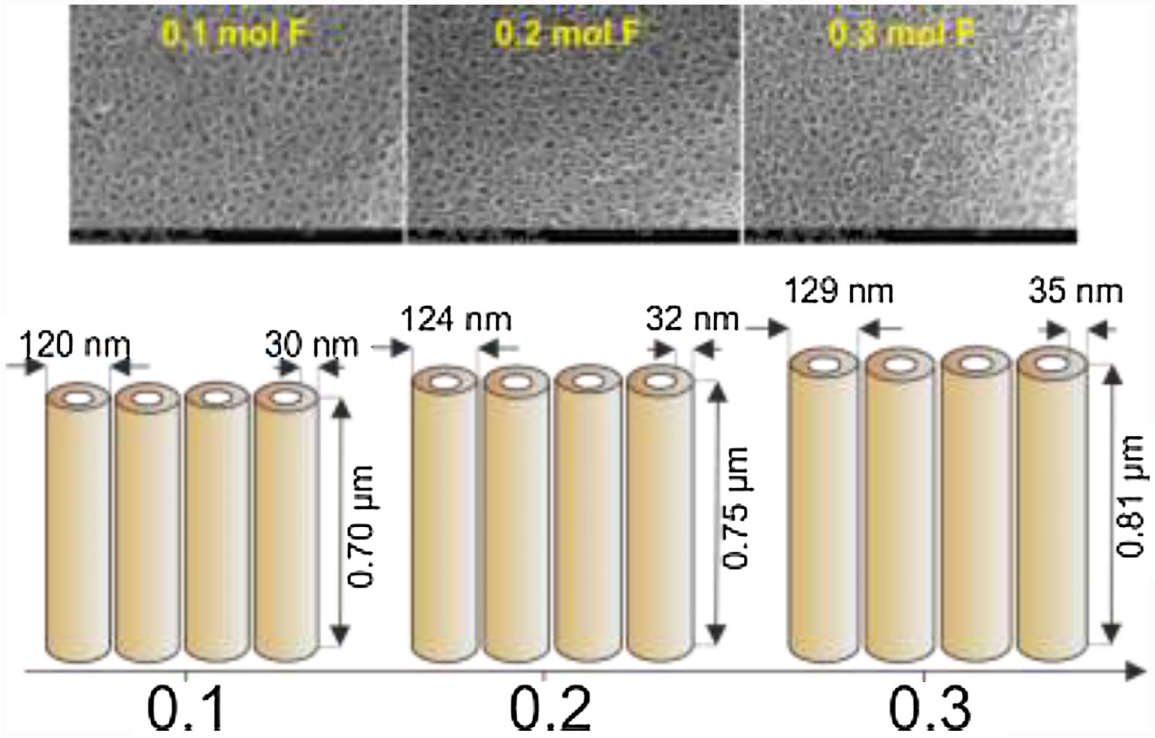

Fig. 5. Effect of the IL content on the morphology of the TiO_2 NTs prepared in the presence of EG/[OMIM][BF_4]-based electrolyte. Water content 10 vol.%, anodization potential 80 V.

3.2.3. Effect of the water content

Effect of water content in the electrolyte was investigated by anodization at 80 V for 20 min in the electrolyte containing 0.1 mol F^- also using [OMIM][BF_4] as a source of F^- anions (Fig. 4). Increase of water content from 0 (NTs _[OMIM]_0%H_2O sample) to 10 vol.% (NTs _[OMIM]_10%H_2O sample) provides longer NTs (up to 0.7 µm), while a further increase in water content up to 15 vol.% (NTs _[OMIM]_15%H_2O sample) results in opposite effect (0.35 µm). Opposite relationships were found during anodization in the EG/[BMIM][BF_4]-based electrolyte [27] and similar in a traditional electrolyte composed of NH_4F and glycerol [36]. Above mentioned opposite effect could be related with the difference in physicochemical characteristics of electrolytes used in our study and work published by Teixeira group [27].

3.2.4. Effect of the ionic liquid content

The results presented in Fig. 5 revealed that the NTs can be elongated by increasing the amount of [OMIM][BF_4], starting with approximately d = 120 nm and l = 0.7 µm (NTs_[OMIM] sample containing 0.1 mol F^-) and reaching approximately d = 129 nm and l = 0.81 µm (NTs_[OMIM]_0.3F^- sample containing 0.3 mol F^-). Similar trends were observed by others when anodization was conducted in EG/[BMIM][BF_4]-based electrolyte [27] and organic electrolytes containing HF or NH_4F [37].

Powder X-ray diffraction patterns of all obtained photocatalysts are presented in Fig. S1. All patterns look similar, with only few X-ray diffraction reflections that were indexed by Ti metal (black vertical bars) and TiO_2 anatase (blue vertical bars). The highest intensity peaks for TiO_2 at 25.4° and 47.8° can be ascribed to (101) and (200) plane, respectively. Estimated lattice parameters, unit cell volume and crystallize size for the anatase phase (space group I41/amd) are gathered in Table 2. The average crystallize size was calculated from the Scherrer formula based on the line broadening at half the maximum intensity of (101) reflection. The results suggest that there is no clear relation between the amount and structure of the IL, applied anodization potential and the lattice parameters as well as the crystallite size. However, increasing water concentration causes decrease in a lattice parameter from 3.8135(9) Å to 3.8001(5) Å, for 0% H_2O and 15 vol.% H_2O, respectively. Since c lattice parameter remains almost unchanged, the unit cell volume decreases from 141.6 $Å^3$ to 140.57 $Å^3$ with increasing H_2O from 0% to 15 vol.% (see Table 2 and Fig. S2). This behavior is likely caused by non-metal (such as boron) incorporation into TiO_2 lattice [38] and due to Ti^{3+} generation [39]. Interestingly the crystallize size increases by a factor of two when water (15 vol.%) was added.

3.3. Chemical composition of the IL-assisted TiO_2 NTs

The coexistence of carbon, nitrogen, fluorine and boron evidenced successful interaction between IL and growing TiO_2 NTs (Table 3, Fig. 6). Deconvoluted spectra (Fig. 6) exhibit features, characteristic for doped TiO_2 NTs. The carbon states at BE close to 286.2 eV, 288.9 eV and 290–293 eV are characteristic for N—C=C—N, N—C=N and C—Fx bonds, respectively [40], whereas the oxygen fraction at BE 531.9 eV can be assigned to Ti—O—N bound. The carbon peak at BE of 286.2 eV represents imidazole-metal bound formed through C4 or C5 carbon in the heterocyclic ring, whereas peak at 288.9 eV can be identified as imidazole-metal bound formed through C2 carbon [17]. The relative contribution of all carbon species revealed by deconvoluted fractions of C 1s spectra is summarized in Table 3 (see fractions "B" and "C").

The broad peak at BE 399.8–400.2 eV can be assigned to coexisting nitrogen states formed by C—NH—C and C=N—C bounds, which are attributed to pyrrole- and pyridine-type interaction [40,41]. The nitrogen state at 400 eV can be formed by various nitrogen compounds, including molecularly adsorbed nitrogen [42,43] as well as Ti—O—N adspecies [44]. The peaks detected at BE higher than 401.7 eV can be ascribed to the positively charged nitrogen (—N+) originated from pyridine–type nitrogen bound and to oxidized form

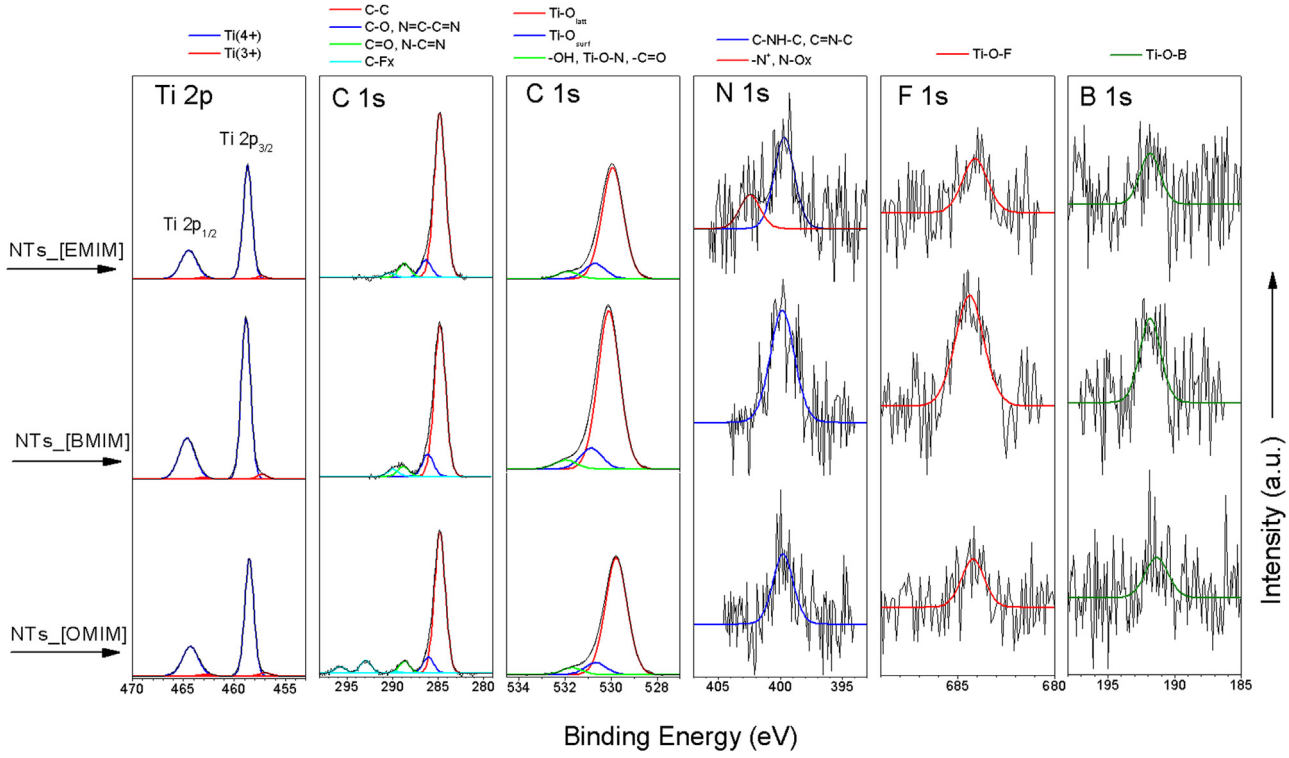

Fig. 6. The Ti2p, O1s, N1s, F1s and B1s spectra, recorded for TiO_2 NTs prepared in the electrolytes contained EG, water and [EMIM][BF_4] or [BMIM][BF_4] or [OMIM][BF_4].

of nitrogen species [43]. Small peaks, at 399.0 eV can be ascribed to Ti-Nx bound [43], forming by nitrogen atoms interaction with TiO_2 matrix.

The F1s and B1s spectra (Fig. 6) were well fitted by one component (BE = 684.7 and 191.7 eV, respectively) and not changed with alkyl chain length. The spectra evidenced the effective interaction between the IL anions and TiO_2 NTs leading to Ti—O—B [45,46] and $TiOF_2$ [47] species formation.

The inspection of XPS data collected in Table 3 revealed that nitrogen content in NTs_[EMIM] sample was estimated to be larger than in corresponding NTs_[BMIM] and NTs_[OMIM] samples. The atomic concentration (AC) ratio N/Ti was found to decrease from 0.013 to 0.008 in a sequence of NTs_[EMIM], NTs_[BMIM] and NTs_[OMIM] samples. Assuming that nitrogen in all TiO_2 NTs originated mainly from the IL interaction, we can conclude that the surface concentration of the IL with shorter alkyl substituent in the imidazolium ring is relatively larger than in corresponding TiO_2 NTs containing the IL with longer substituent. Thus, the lowest coverage of the [OMIM] ions can be resulted of larger steric effect induced by that cation. The AC ratios C/N, evaluated for all samples, were estimated to be much larger than nominal values related to corresponding IL ions (see Table 3). This suggests that carbon species can be originated not only from preparation process but additional carbon contaminants.

The formation of NTs was found to be sensitive to the water content in the electrolyte (Fig. S3 and Table 3). It is interesting to note that the AC ratio N/Ti, estimated for samples formed with water content 0 and 15 vol.%, was found to be larger than corresponding values for samples formed with water content 2.5 and 5 vol.%. At the same time the AC ratio B/N for samples formed with water content 0 and 15 vol.%, was smaller than for samples formed with water content 2.5 and 5 vol.%. This trend is in line with morphological data reported above. No effect of different anodization potential applied during IL-assisted synthesis of TiO_2 NTs was observed (Fig. S4 and Table 3). The HR spectra of elements detected at surface areas of these samples revealed the similar chemical character and no clear relation between applied anodization potential and the surface composition was found. However, the systematic changes in the surface composition can be observed for the samples prepared using different amount of IL in the electrolyte. One can see that the AC ratios F/Ti and N/Ti increased as the amount of fluoride increases from 0.1 to 0.3 mol F^- (Fig. S5 and Table 3).

3.4. *Mechanism of the IL-assisted formation of TiO_2 NTs*

Based on the experimental results presented above (XPS analyses) and literature data, a probable formation mechanism of IL-NTs was proposed and is shown in Fig. 7. Considering the points in the above discussion, the nonmetal elements like B and N may originate from the partial hydrolysis/decomposition of [BF_4] and the imidazolium cation and are simultaneously introduced into the obtained IL-NTs. It is known that the [BF_4]-based ILs hydrolyze in the presence of water not only in acidic/basic conditions and at elevated temperatures but even at room temperatures [48]. Hydrolyzed solutions of imidazolium tetrafluoroborate may contain hydrofluoric and boric acid as well as fluoroboric acid whereas the imidazolium cation remains unchained [49]. The presence of boron compounds in the electrolyte allows the introduction of B element into the TiO_2 bulk, as it already was shown in [50,51]. Furthermore, the XRD results revealed that the lattice parameters remain almost unchanged along the a- and b-axes while the c-axis parameter changes, which also confirms the presence of B in the TiO_2 bulk. The presence of F^- (because of partial hydrolysis) and [BF_4] anions in the reaction environment may further result in the formation of water-soluble $[TiF_6]^{2-}$ and $[Ti(BF_4)_6]^{2-}$ species *via* chemical attack of the formed TiO_2 according to the reaction presented in Fig. 7. Formation of the water-soluble $[TiF_6]^{2-}$ [52] and $[Ti(BF_4)_6]^{2-}$ [26] species allows the growth of a tabular structure. Notably, the presence of fluoride (detected by XPS) on the surface of NTs can be derived from adsorbed $[TiF_6]^{2-}$ and $[Ti(BF_4)_6]^{2-}$ species. To gain insight

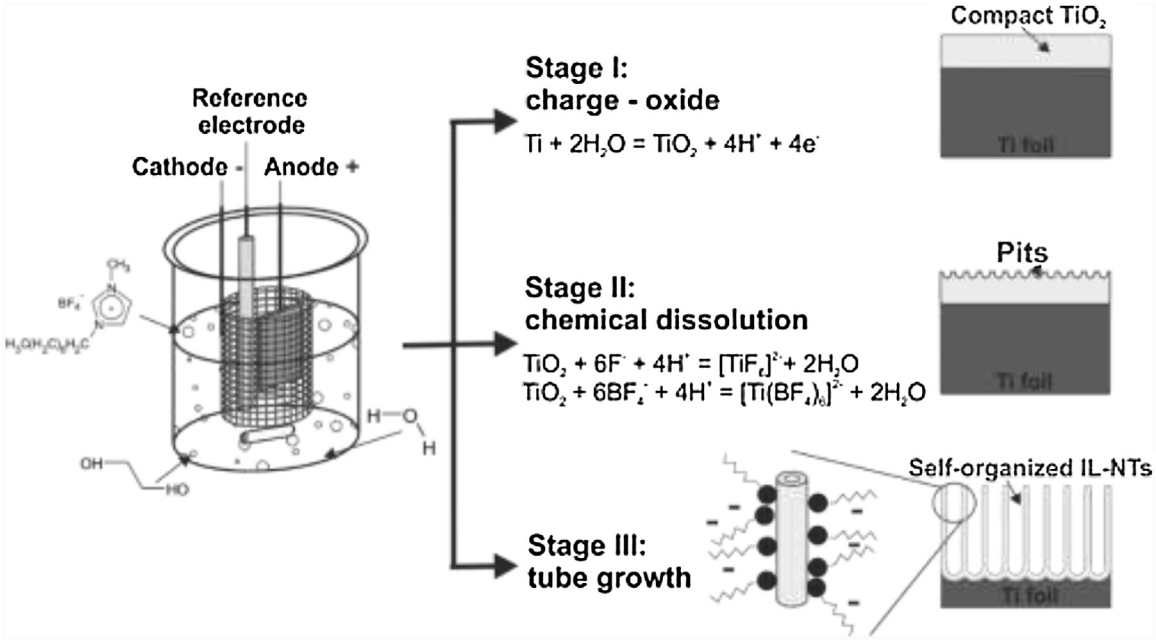

Fig. 7. Formation mechanism of the IL-NTs obtained by anodization of Ti in the EG/IL-based electrolytes.

into the origin of the N atoms introduced to the TiO_2 lattice, we investigated the electrolyte composition ([OMIM][BF_4], 10 vol.% of H_2O, 0.1 mol F^-, 80 V), used for NTs_[OMIM] sample preparation, before and after anodization by using HPLC. It was found that the IL concentration in the electrolyte after anodization decreased by approximately 15% compared to IL concentration in the electrolyte before anodization. Furthermore, small peaks (in the electrolyte after anodization), which can be ascribed to products of imidazolium cation decomposition, were also observed. It suggests that N atoms in the TiO_2 bulk may come also from partial decomposition of the imidazolium cation, which occurs during anodization.

Furthermore, although C2 atom is the most acidic, it was observed that all three C atoms are equally involved in formation of the interactions between imidazolium cation and TiO_2 surface since contribution of the "B" and "C" state in carbon fraction (XPS results) is similar (Table 3). In this regard, we can conclude that IL interact preferentially by the charge moieties of the imidazolium cation, which may be oriented close to the surface normal or parallel to the surface with side chains directed away from the surface. The longer the chain length in the imidazolium cation, the larger steric hindrance is created, and this structural determinant results in greater distances between parallelly set NTs observed for tubes obtained in the presence of [OMIM][BF_4] (Fig. 2).

As mentioned previously and presented in Fig. 2, anodization of the Ti substrate in the electrolyte containing the IL with longer alkyl substituent in the imidazolium cation provides better separated, longer NTs with larger outer and inner diameter. As presented in Table 1, application of the IL with longer alkyl substituent in the imidazolium cation resulted in increase of the conductivity of the EG/IL- based electrolytes. In general, higher conductivity of electrolytes enhances the growth rate of NTs, as it facilitates the passage of the current required to form the oxide [53]. On the other hand, the longer the alkyl chain length, the larger the susceptibility of the anion to hydrolysis due to the lower cation-anion interaction strength [49]. Thus, the higher concentration of $[TiF_6]^{2-}$ and $[Ti(BF_4)_6]^{2-}$ species should be expected, which consequently leads to an increase in the NTs dimensions, as presented in Fig. 2 and Table 2 (in the optimal range of fluorine concentration).

3.5. Photocatalytic activity

Photodegradation of phenol aqueous solution is commonly used as standard reaction to estimate photocatalytic properties in the oxidation pathway due to toxicity of this xenobiotic towards higher organisms. This model reaction was used to investigate the effect of the IL structure (chain length in the imidazolium cation) and content, amount of water in the reaction system and anodization potential on the NTs photoactivity. The obtained results indicated that preparation conditions affected the UV–vis ($\lambda > 350$ nm) and Vis light-induced ($\lambda > 420$ nm) photoactivity. The photocatalytic oxidation pathways of organic pollutants usually involve one or more radicals among which •OH is frequently assigned as the crucial one [54]. The hydroxyl radical is one of the most chemically reactive species providing organic pollutant degradation due to strong oxidizing properties [55]. In this regard formation of hydroxyl radicals on the surface of the UV–vis and Vis-illuminated TiO_2 NTs was elucidated by fluorescence (FL) indirect technique using terephthalic acid as a trapping agent. No FL peak was observed in the absence of the photocatalyst under both irradiation sources suggesting that fluorescence is solely due to reaction of terephthalic acid with •OH formed at the TiO_2/water interface via the photocatalytic reactions. The terephthalic acid is known to readily capture •OH forming highly fluorescent 2-hydroxyterephtalic acid in alkaline conditions. Indeed, a peak localized around 425 nm (see insets in Fig. 8) was observed indicating formation of the •OH that react with scavenger giving proper hydroxy derivative. The photocatalytic activity of the ILs-TiO_2 NTs under both UV–vis and Vis light is presented in Fig. 8 and in Table 2 (presented as the reaction rates for 60 min of irradiation).

3.5.1. Effect of the ionic liquid's cation structure

It was observed that length of the alkyl substituent in the IL cation determine both UV–vis as well as Vis light-induced photoactivity, however with different intensity (see Fig. 8a and b). Nevertheless, for both irradiation sources, analogous relation was detected, that is the longer the chain length, the higher photodegradation activity. Phenol degradation rate under UV–vis irradiation increased from 1.0 to 1.56 $\mu mol\,dm^{-3}\,min^{-1}$ as detected after 60 min of experiment for NTs_[EMIM] and NTs_[OMIM], respec-

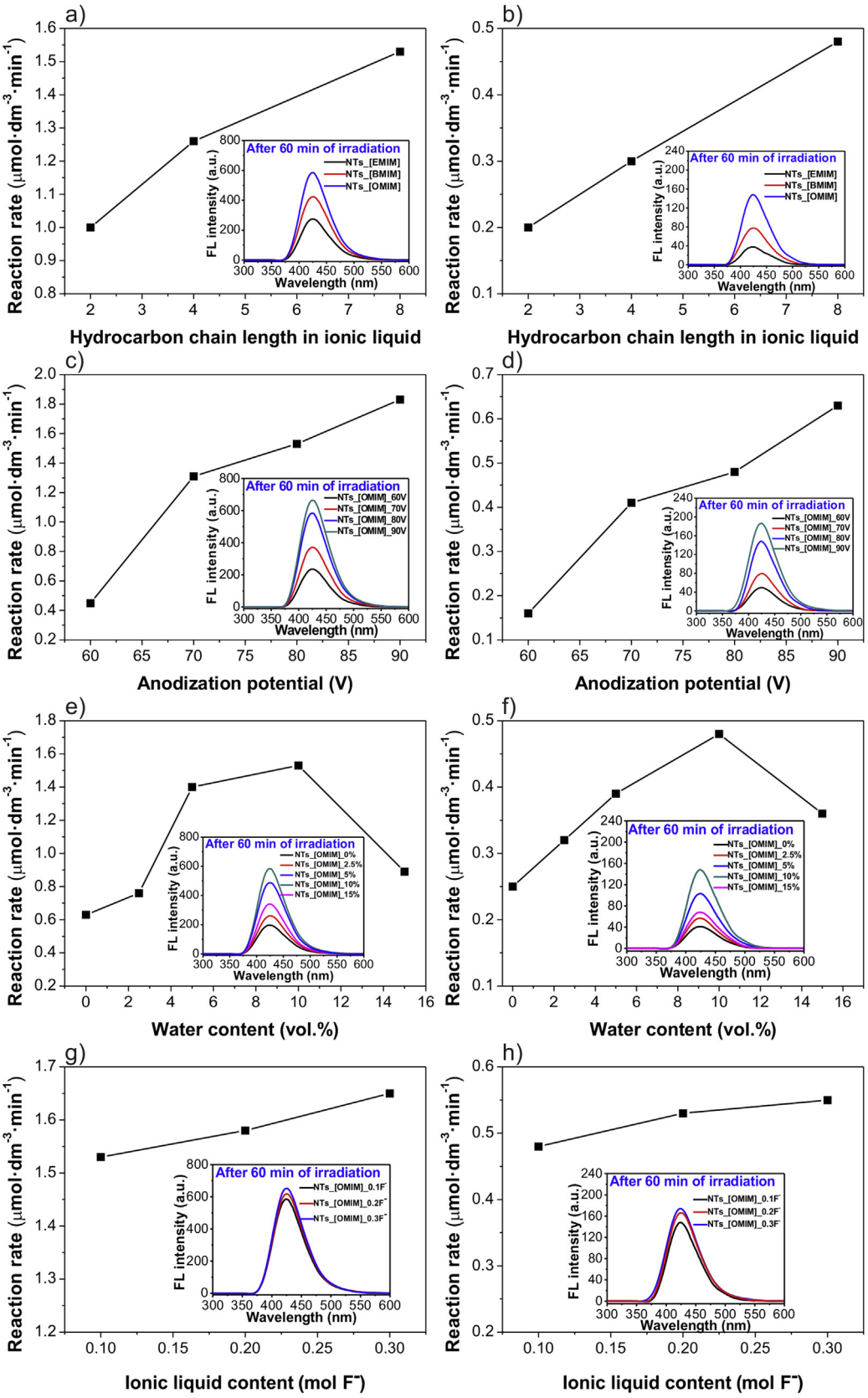

Fig. 8. Photocatalytic properties of IL-NTs under UV (left panel) and Vis irradiation (right panel). Effect of the (a, b) IL's cation, (c, d) anodization potential, (e, f) water content and (g, h) IL content.

Table 3
Elemental composition (in at.%) and chemical characters of titanium, oxygen and carbon states in the surface layer of TiO_2 NTs, evaluated by XPS analysis.

Sample	Ti fraction (%)			O fraction (%)			C fraction (%)						The atomic concentration (AC) ratios				
	$\sum_{(at.\%)}^{Ti}$	Ti^{4+} 458.7 ± 0.1 eV	Ti^{3+} 457.2 ± 0.1 eV	$\sum_{(at.\%)}^{O}$	"A" Ti—O_{latt} 529.9 ± 0.1 eV	"B" Ti—O_{surf} 530.9 ± 0.1 eV	"C" —OH, —C=O, Ti—O—N, 531.9 ± 0.1 eV	$\sum_{(at.\%)}^{C}$	"A" C—C 284.8 eV	"B" C—OH, N—C=C—N 286.2 ± 0.1 eV	"C" —C=O, N—C=N 288.9 ± 0.2 eV	"D" —C—Fx 290–293 eV	$\sum_{(at.\%)}^{N}$	$\sum_{(at.\%)}^{F}$	$\sum_{(at.\%)}^{B}$	F/Ti	B/Ti	N/Ti	C/N	B/N
NTs_[EMIM]	24.07	97.23	2.77	56.45	82.98	11.54	5.48	18.63	81.75	8.88	7.06	2.31	0.31	0.19	0.35	0.008	0.015	0.013	60.1	1.13
NTs_[BMIM]	25.96	96.67	3.33	59.99	83.86	11.24	4.90	12.99	79.49	11.63	5.18	3.69	0.29	0.33	0.44	0.013	0.017	0.011	44.8	1.52
NTs_[OMIM]	25.29	96.46	3.54	58.90	85.80	8.98	5.22	15.14	76.90	8.83	6.57	7.91	0.20	0.15	0.32	0.006	0.013	0.008	75.7	1.60
NTs_[OMIM]_60V	24.25	96.98	3.02	57.73	85.52	9.94	5.53	17.23	84.48	5.60	6.84	3.08	0.39	0.13	0.27	0.005	0.011	0.016	44.2	0.69
NTs_[OMIM]_70V	21.55	96.55	3.45	52.30	84.14	8.99	6.87	25.32	85.88	7.05	3.84	3.23	0.34	0.14	0.35	0.006	0.016	0.016	74.5	1.03
NTs_[OMIM]_90V	24.51	96.64	3.36	57.90	86.69	8.28	5.03	16.71	83.86	6.04	8.10	2.00	0.28	0.26	0.34	0.011	0.014	0.011	59.7	1.21
NTs_[OMIM]_0%H_2O	21.58	96.04	3.96	51.27	84.84	8.68	6.48	26.18	88.91	4.78	4.78	1.54	0.37	0.22	0.36	0.010	0.017	0.017	70.8	0.97
NTs_[OMIM]_2.5%H_2O	26.00	96.19	3.81	60.13	83.24	11.60	5.16	12.79	75.71	12.34	10.05	1.90	0.21	0.36	0.50	0.014	0.019	0.008	60.9	2.38
NTs_[OMIM]_5%H_2O	25.93	96.66	3.34	59.82	83.11	11.82	5.07	13.38	79.07	9.99	8.30	2.64	0.20	0.27	0.39	0.010	0.015	0.008	66.9	1.95
NTs_[OMIM]_15%H_2O	24.64	96.77	3.23	56.54	85.38	9.82	4.79	17.91	83.93	8.99	5.70	1.38	0.37	0.25	0.29	0.010	0.012	0.015	48.4	0.78
NTs_[OMIM]_0.2F^-	24.46	95.84	4.16	56.33	92.80	1.32	5.87	18.57	83.79	7.43	6.50	2.27	0.26	0.17	0.22	0.007	0.009	0.011	71.4	0.85
NTs_[OMIM]_0.3F^-	23.95	96.60	3.40	54.65	84.85	9.98	5.17	20.37	83.07	9.55	6.09	1.30	0.37	0.37	0.28	0.015	0.012	0.015	55.1	0.76

tively. Photocatalytic degradation rate under Vis irradiation, in turn, increased from 0.2 to 0.48 μmol dm^{-3} min^{-1} for NTs_[EMIM] and NTs_[OMIM], respectively. The intensity of the FL peak is proportional to the amount of •OH produced, therefore gradual increase in FL intensity at 425 nm was observed with increasing alkyl chain length at the imidazolium cation of the IL used for NTs synthesis under both UV–vis and Vis irradiation. This observation confirms the highest photocatalytic efficiency of TiO_2—NTs prepared in the presence of [OMIM][BF_4], whereas the lowest when [EMIM][BF_4] was used. Comparing FL intensity at 425 nm for experiments carried out under UV–vis and Vis irradiation, as it was expected, the higher •OH generation at the surface of illuminated photocatalysts was detected for the former conditions.

3.5.2. Effect of the anodization potential

To observe the effect of the anodization potential on the photoactivity, series of NTs was prepared in the EG/[OMIM][BF_4]-based electrolyte, and the results are shown in Fig. 8c and d. It was found that the photocatalytic degradation of phenol under the influence of both UV–vis and Vis light irradiation over IL-NTs depended on the anodization potential. In the case of the UV–vis irradiation, the photocatalytic degradation rate increased from 0.45 (NTs _[OMIM]_60 V) up to 1.8 μmol dm^{-3} min^{-1} detected for NTs _[OMIM]_90 V. Similarly, as for UV–vis irradiation, photocatalytic degradation rate under Vis irradiation enhanced with increasing anodization potential, reaching 0.63 μmol dm^{-3} min^{-1} for samples anodized at 90 V (NTs _[OMIM]_90 V). Furthermore, from the insets in Fig. 8c and d, it is evident that the amount of OH radicals produced under both UV–vis and Vis irradiation increased with increasing anodization potential. Thus, the same relationship was observed for both reaction systems: phenol degradation and OH radicals generation.

3.5.3. Effect of the water content

The correlation between the water content and photoactivity was studied using NTs prepared in the presence of EG/[OMIM][BF_4]-based electrolyte, and the obtained results are shown in Fig. 8e and f. From the observations of the reaction rates under UV–vis and Vis irradiation, the NTs_[OMIM] prepared in the electrolyte composed of 10 vol.% of water had the highest photoactivity (1.53 and 0.48 μmol dm^{-3} min^{-1}, respectively) among the series. However, further increase of the water content up to 15 vol.% (NTs_[OMIM]_15%H_2O) resulted in the opposite effect. Thus, after 60 min of irradiation, the phenol degradation rate was 0.89 (UV–vis light) and 0.36 μmol dm^{-3} min^{-1} (Vis light). The same dependence was found for second reaction system, namely generation of •OH radicals under both UV–vis and Vis irradiation, as shown in inserts in Fig. 8e and f. The highest phenol degradation rate and greatest amounts of generated •OH radicals were observed for NTs_[OMIM] prepared in the electrolyte composed of 10 vol.% of water. Similarly, a sample which has the weakest ability to degrade phenol, exhibited the lowest amount of generated •OH radicals.

3.5.4. Effect of the ionic liquid content

The effect of fluoride content in the EG/[OMIM][BF_4]-based electrolytes on the photoactivity under UV–vis and Vis irradiation is presented in Fig. 8g and h. The phenol degradation rate increased as the fluoride content increased, reaching for NTs_[OMIM]_0.3F^- sample 1.65 and 0.55 μmol dm^{-3} min^{-1} for UV–vis and Vis irradiation, respectively. Moreover, a close correlation was observed between efficiency of phenol degradation and OH radicals formation. Sample NTs_[OMIM]_0.3F^- exhibited the highest efficiency of phenol degradation and generation of OH radicals, under both UV–vis and Vis irradiation, respectively. It should be noted that the linear relationship between the fluorescence intensity and

irradiation time confirmed the excellent stability of the obtained photocatalysts.

3.6. Discussion of photocatalytic activity mechanism

Based on the literature date [56,57] and our experience [29,58], the length of IL-NTs as that is the most important geometrical parameter that should be considered during the discussion of photoactivity under UV–vis irradiation. The difference in length of IL-NTs was achieved by varying e.g. anodization voltage in the range of 60–90 V. Notably, the photocatalytic reaction rate increased linearly from 0.45 to 1.82 μmol dm^{-3} min^{-1} with the length of tubes increasing from 0.2 to 0.85 μm (see Table 2). Additionally, similar trends were observed by changing the fluoride concentration and ionic liquid cation in the EG/IL-based electrolyte, namely, increase of NTs' length from 0.70 to 0.81 and from 0.35 to 0.70 μm led to increase of photocatalytic reaction rate from 1.53 to 1.65 and from 1.0 to 1.53 μmol dm^{-3} min^{-1}, respectively. As expected, the highest photocatalytic degradation rate under UV–vis irradiation (1.82 μmol dm^{-3} min^{-1}) as well as the highest efficiency of the hydroxyl radical formation were observed for the NTs with the highest length (0.85 μm). These results correspond well with other reports in the literature. Macak et al. [59] suggested that photoactivity of NTs under the influence of UV irradiation depends on the length of NTs, namely the longer length, the higher is photocatalytic activity due to reduced recombination of photogenerated charge carriers and more efficient light absorption. Another studies confirm these results, especially, Liu et al. [56] who showed that degradation rate constant of acetaldehyde depended on the length of TiO_2 NTs, which increased from 0.011 to 0.018 min^{-1} with increasing the length of NTs from 8.4 to 17 μm, respectively. Zhuang et al. [60], who studied effect of the NTs' length (0.4–3.5 μm) on the photocatalytic decomposition of methyl orange, observed a maximal photoactivity (0.177 min^{-1}) in the presence of 2.5 μm-long NTs. Kontos et al. [57], in turn, examined the influence of TiO_2 NTs length on the photoactivity in the gas phase and found that degradation of toluene and benzene (at ppb concentrations) increased with increasing the length of NTs. Furthermore, similar observations were performed for NTs prepared in EG/[BMIM][BF_4]-based electrolyte, where photocatalytic degradation of methyl orange was higher for sample which had longer tube [27].

The sample that exhibited the highest photocatalytic activity under UV–vis irradiation (1.82 μmol dm^{-3} min^{-1}) was NTs_[OMIM]_90V prepared at anodization potential 90 V in the electrolyte containing 0.1 mol of [OMIM][BF_4] (represented by F^- content) and 10 vol.% of water. Analogously, the highest photocatalytic degradation rate under Vis irradiation (0.63 μmol dm^{-3} min^{-1}) as well as the highest efficiency of the hydroxyl radical formation were also observed for the same sample. This was the longer sample (0.85 μm) consisted of 24.48 at.% of Ti (3.36 at.% of which were Ti^{3+}), 57.82 at.% of O, 16.69 at.% of C, 0.30 at.% of N, 0.26 at.% of F, and 0.46 at.% of B. As previously explained, boron and nitrogen elements are incorporated into TiO_2 lattice. According to the literature date and our previous work, the ncorporation of nonmetals, such as boron and nitrogen, into the TiO_2 lattice leads to the formation of a new energy state, namely, he N 2p and B 2p band above the O 2p valence band, which may decrease the band gap of TiO_2 and shifts the optical absorption o the visible light region [61]. Therefore, it is possible for the electrons to migrate from the valence band to the conduction band upon absorbing visible light, which leads to the visible light photoactivity of as-obtained IL-NTs. Based on the presented results, possible pathway can be considered to explain the photocatalytic mechanism over IL-NTs under visible light, as shown in Fig. 9a. At his point it should be noted that the as-prepared samples had the arge amount of Ti^{3+} (see Table 3) compared to NTs prepared in the traditional electrolytes [58]. Thus, their role in the excitation mechanism under Vis light should be considered since oxygen vacancies enhances the visible light response [62]. Optical absorption properties of NTs_[EMIM], NTs_[BMIM] and NTs_[OMIM] samples are shown in Fig. S6a. Obtained results confirm improved visible light absorption, which is characteristic for photocatalysts possessing Ti^{3+} species [63]. Thus, electrons in the conduction band (or in the Ti^{3+} states) react with oxygen molecules dissolved in water, to produce oxidative species, such as superoxide radical anions and in the next stage hydroxyl radicals. At the same time, the holes photogenerated in the valance band (or in the localized dopant levels) react with OH^- ions to generate highly oxidative species, hydroxyl radicals. The synergistic effect of N 2p and B 2p states and Ti^{3+} states may further reduce the photon excitation energy from the VB to the CB under visible-light irradiation, which leads to an enhancement of the visible photocatalytic activity [62]. In addition, presence of the IL on the TiO_2 NTs surface cannot result in absorption of the visible photons because the band gaps of used ionic liquids are too wide (more than 6 eV) [64].

Under UV–vis irradiation, N, B and Ti^{3+} species incorporated into TiO_2 matrix can facilitate electron–hole separation and promote the interfacial electron transfer process [61,63].

Under both UV–vis and Vis irradiation, photogenerated electrons react with O_2 to form the $O_2^{\bullet-}$ superoxide radical (E^0 ($O_2/O_2^{\bullet-}$) = −0.33 V_{SHE}), according to the following reaction:

$$O_2 + e^- \rightarrow O_2^{\bullet-} \quad (1)$$

Notably, $O_2^{\bullet-}$ species are very reactive and can oxidize molecules and transform into hydroxyl radicals through the following reactions:

$$O_2^{\bullet-} + H^+ \rightarrow HO_2^{\bullet} \quad (2)$$

$$2HO_2^{\bullet} \rightarrow H_2O_2 + O_2 \quad (3)$$

$$O_2^{\bullet-} + H_2O_2 \rightarrow {}^{\bullet}OH + O_2 + HO^- \quad (4)$$

$$H_2O_2 + h\nu \rightarrow 2HO^{\bullet} \quad (5)$$

While in the valance band, the photogenerated holes can react with H_2O to yield strong $HO^{\bullet}$ radicals (E^0 ($^{\bullet}OH/H_2O$) = +2.27 V_{SHE}):

$$H_2O + h^+ \rightarrow {}^{\bullet}OH + H^+ \quad (6)$$

According to literature data, content of dopant, Ti^{3+} species, —OH groups and crystallites size belong to the most important parameters having the greatest effect on the photocatalytic properties of non-metal doped TiO_2 photocatalysts under Vis irradiation. Therefore, there is an optimal amount of these species promoting high photocatalytic activity [60,65–67]. Considering discussed IL-NTs which exhibited different length, the most photoactive sample under Vis irradiation met the following conditions: low concentration of carbon impurities (16.69 at.%), high amount of Ti^{3+} forms (0.82 at.%), optimal (relatively low) crystallites' size (36 nm) and medium dopant content (0.30 and 0.46 at.% for nitrogen and boron, respectively) and the highest NTs length. Additionally, there is also optimal length of doped-NTs that exhibited the highest photocatalytic performance under Vis light [58]. Under Vis irradiation, when the NTs layer is thicker than the penetration depth of light, the bottom part of the NTs probably absorbs only small amount of incident photons and acts only as an inter-support. On the other hand, the mass transfer can be limited by a longer diffusion pathway, which consequently leads to a decrease in the photocatalytic degradation rate. Zhuang et al. [60] explained that, the absorption of photons and adsorption of organic pollutants increases with the increase of TiO_2 NTs thickness, which is advantageous for photocatalytic process. In summary, rather, the combination of above mentioned parameters has the greatest impact on the photoactivity. Noticeably, the presence of IL at the NTs surface can also

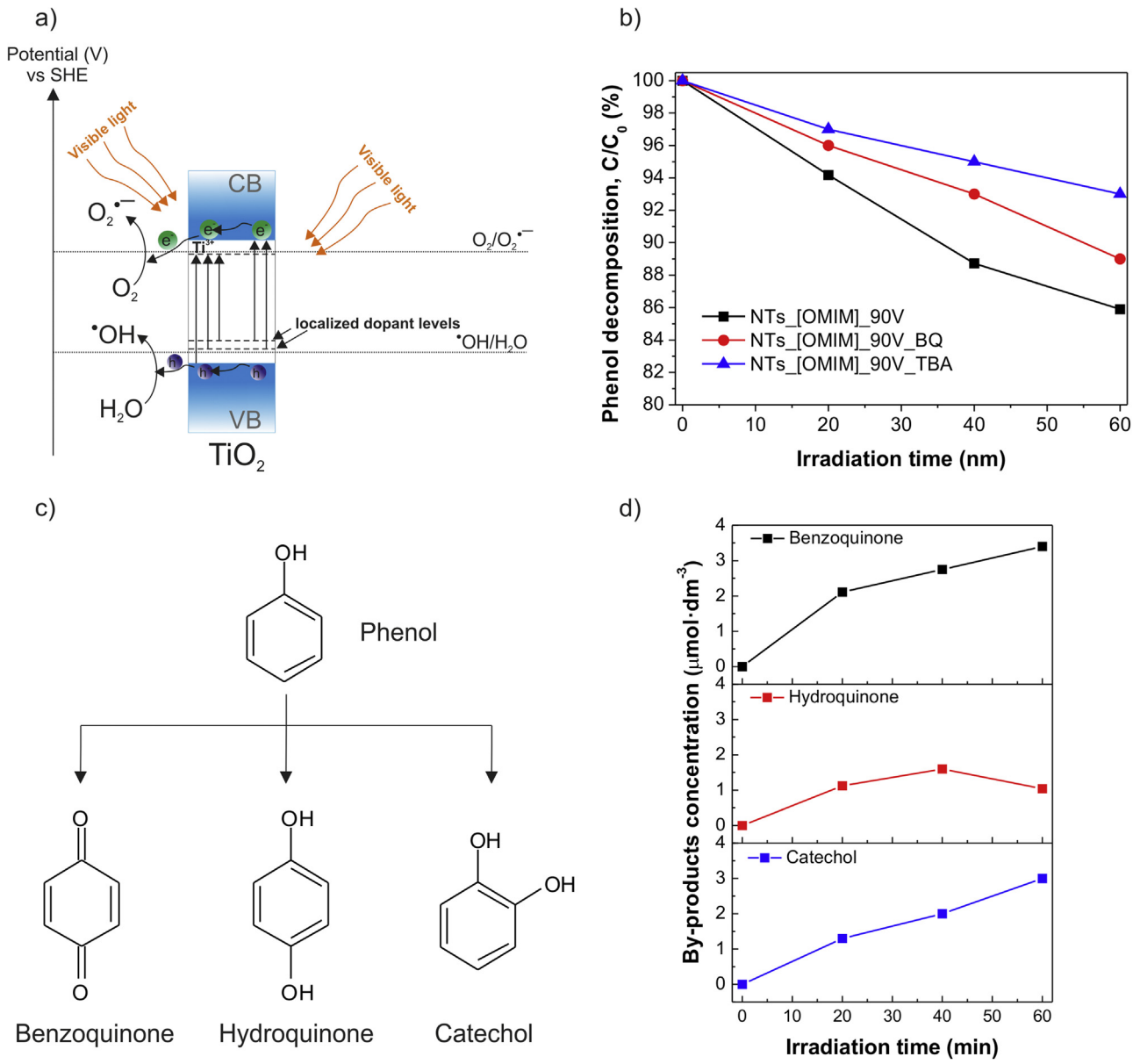

Fig. 9. (a) Proposed photocatalytic mechanism over IL-NTs under visible light irradiation and (b) photocatalytic decomposition of phenol under visible light irradiation in the presence of scavengers (BQ – benzoquinone; TBA – *tert*-butyl alcohol), (c) chemical structures of intermediates formed during phenol irradiation and (d) evolution of primary intermediates upon Vis light in the presence of the NTs_[OMIM]_90 V sample.

markedly enhance the charge separation of photogenerated carriers at the photocatalysts surface and, as a consequence, increased photocatalytic activity [17].

To better understand the role of active species in the process of photocatalytic phenol degradation under Vis irradiation, photocatalytic degradation of phenol in the presence of selected sample (NTs_[OMIM]_90V) and different scavengers was performed. According to the literature date, $O_2^{\bullet-}$ and •OH radicals are the most important oxidative species which possesses the highest oxidation potentials [68]. To determinate the role of the generated oxidative species in the photocatalytic process under Vis irradiation, *tert*-butanol and benzoquinone were used as scavengers of hydroxyl and $O_2^{\bullet-}$ radicals, respectively. As shown in Fig. 9b, the presence of each scavenger separately caused the significant decrease of phenol decomposition efficiency (decreased by approximately 4 and 8% in the presence of the superoxide and hydroxyl radicals scavengers, respectively). These results confirm the crucial role of •OH and $O_2^{\bullet-}$ radicals in the photocatalytic process of phenol degradation under both UV–vis and Vis irradiation.

To determinate the photostability of the most photoactive sample (NTs_[OMIM]_90 V), the phenol degradation reactions in four subsequent cycles were performed, and results are shown in Fig. S6b and c. From the observation of degradation rates, the obtained IL-NTs exhibited photostability. Phenol degradation rate remained at level about 1.50 and 0.42 μmol dm^{-3} min^{-1} after 60 min of UV–vis and Vis irradiation after four cycles. Howeover, under UV–vis irradiation, sample (NTs_[OMIM]_90 V) had slightly better photostability compared to Vis light, which may be related to its better photoactivity in first measurement cycle (higher degradation rate) and consequently with better efficiency in phenol degradation byproducts removal. Furthermore, the durability of obtained sample (NTs_[OMIM]_90 V) under both UV–vis and Vis irradiation has been tested through the following procedure: firstly, sample was used in phenol decomposition process and then used sample was irradiated by UV lamp (in air, to clean the surface), and then

re-use in phenol degradation reaction (this procedure was applied four times). Phenol degradation efficiency under UV–vis and Vis remained almost unchanged after four times re-use, which suggests that obtained photocatalysts exhibited the high durability.

Additionally, to follow the intermediates formation under Vis irradiation, high performance liquid chromatography was applied and results are presented in Fig. 9c and d. Photocatalytic degradation measurements conducted over NTs_[OMIM]_90V sample under Vis irradiation indicated that catechol, hydroquinone and benzoquinone were detected and determined quantitatively as the intermediates formed during phenol photodegradation under Vis irradiation. According to literature date [69], these dihydroxybenzenes belong to primary products of the photodegradation, which can easily be detected using HPLC. The ring-opening products could not be identified by HPLC [70,71]. Moreover, it was found that concentration of catechol and benzoquinone increased during the irradiation process, while hydroquinone content began to decrease after 40 minut of irradiation (see Fig. 9d), which suggests phenol mineralization.

4. Conclusions

Well-aligned, active under Vis irradiation TiO_2 NTs were obtained through simple and environmentally friendly one-step anodization of the Ti foil in solutions containing ethylene glycol, water and $[BF_4]$-bearing ionic liquids with different chain length in the imidazolium cation. Ionic liquids served both as a source of fluorine ions (crucial for nanotubes formation), as well as, a source of nonmetal elements (such as nitrogen and boron), which could be incorporated into TiO_2 structure during nanotubes formation. This facile method enables grow of TiO_2 NTs in a form of nanoporous thin film ready to use without necessity to separate from the reaction environment.

It was found that IL structure and its content allows to control the morphological features and, as a consequence, photoactivity of TiO_2 NTs. The EG/[OMIM][BF_4]-based electrolyte turned out to be more promising reaction medium compared to previously known electrolyte based on [BMIM][BF_4]. An increase of the NT length (from 0.35 to 0.7 μm) and diameter (from 100 to 120 nm) was found when [EMIM][BF_4] was replased with [OMIM][BF_4] ionic liquid. The sample that exhibited the highest photocatalytic activity under UV–vis and Vis irradiation (1.8 and 0.63 $\mu mol\, dm^{-3}\, min^{-1}$, respectively) as well as the highest efficiency of the hydroxyl radical formation was TiO_2—NTs prepared at anodization potential 90 V in the electrolyte containing 0.1 mol of [OMIM][BF_4] (represented by F^- content) and 10 vol.% of water. Performance improvement under Vis irradiation occurs as a result of the nitrogen, boron and Ti^{3+} incorporation into TiO_2 bulk due to partial decomposition of imidazolium cation and hydrolysis of [BF_4^-]. Furthermore, the photocatalytic activity under Vis irradiation was found to be attributable not only to •OH but also to other forms of reactive oxygen species, such as $O_2^{\bullet -}$, H_2O_2 and HO_2• radicals. In this regard, the obtained photocatalysts meet the specifications for use in various photocatalytic applications due to their large surface area, activity in Vis light and stability. Further studies designed to increasing the length of the NTs can prove great potential for commercial applications.

Acknowledgments

The author J.Ł. acknowledges funding from the National Science Center within program SONATA 8 (grant entitled: "Influence of the ionic liquid structure on interactions with TiO_2 particles in ionic liquid assisted hydrothermal synthesis", contract No. 2014/15/D/ST5/0274. The authors A.Z.M. and P.M. acknowledge funding from the National Science Centre within program OPUS 8 (grant entitled: Ordered TiO_2/M_xO_y nanostructures obtained by electrochemical method, contract No.: 2014/15/B/ST5/00098), for work described here.

Appendix A. Supplementary data

Supplementary data associated with this article can be found, in the online version, at http://dx.doi.org/10.1016/j.apcatb.2017.05.005.

References

[1] X. Chen, S.S. Mao, Titanium dioxide nanomaterials: synthesis, properties, modifications, and applications, Chem. Rev. 107 (2007) 2891–2959.
[2] U. Diebold, The surface science of titanium dioxide, Surf. Sci. Rep. 48 (2003) 53–229.
[3] Y. Xia, P. Yang, Y. Sun, Y. Wu, B. Mayers, B. Gates, Y. Yin, F. Kim, H. Yan, One-dimensional nanostructures: synthesis, characterization, and applications, Adv. Mater. 15 (2003) 353–389.
[4] M. Nischk, P. Mazierski, Z. Wei, K. Siuzdak, N.A. Kouame, E. Kowalska, H. Remita, A. Zaleska-Medynska, Enhanced photocatalytic, electrochemical and photoelectrochemical properties of TiO2 nanotubes arrays modified with Cu AgCu and Bi nanoparticles obtained via radiolytic reduction, Appl. Surf. Sci. 387 (2016) 89–102.
[5] P. Mazierski, J. Nadolna, W. Lisowski, M.J. Winiarski, M. Gazda, M. Nischk, T. Klimczuk, A. Zaleska-Medynska, Effect of irradiation intensity and initial pollutant concentration on gas phase photocatalytic activity of TiO2 nanotube arrays, Catal. Today 284 (2017) 19–26.
[6] P. Mazierski, A. Malankowska, M. Kobylański, M. Diak, M. Kozak, Winiarski, MJ, T. Klimczuk, W. Lisowski, G. Nowaczyk, A. Zaleska-Medynska, Photocatalytically active TiO2/Ag2O nanotube arrays interlaced with silver nanoparticles obtained from the one-step anodic oxidation of Ti-Ag alloys, ACS Catal. 7 (2017) 2753–2764.
[7] P. Roy, D. Kim, K. Lee, E. Spiecker, P. Schmuki, TiO2 nanotubes and their application in dye-sensitized solar cells, Nanoscale 2 (2010) 45–59.
[8] J. Łuczak, M. Paszkiewicz, A. Krukowska, A. Malankowska, A. Zaleska-Medynska, Ionic liquids for nano- and microstructures preparation. Part 1: properties and multifunctional role, Adv. Colloid Interface Sci. 230 (2016) 13–28.
[9] J. Łuczak, M. Paszkiewicz, A. Krukowska, A. Malankowska, A. Zaleska-Medynska, Ionic liquids for nano- and microstructures preparation. Part 2: application in synthesis, Adv. Colloid Interface Sci. 227 (2016) 1–52.
[10] J. Dupont, J.D. Scholten, On the structural and surface properties of transition-metal nanoparticles in ionic liquids, Chem. Soc. Rev. 39 (2010) 1780–1804.
[11] Z. He, P. Alexandridis, Nanoparticles in ionic liquids: interactions and organization, Phys. Chem. Chem. Phys. 17 (2015) 18238–18261.
[12] Y. Yu, Y. Jiang, M. Tian, L. Yang, H. Yan, S. Sheng, N-doped TiO2 nanotube arrays: synthesis by anodization in an ionic liquid ([BMIM] BF 4) and assessment of photocatalytic property, Rare Metal Mater. Eng. 45 (2016) 561–566.
[13] S. Yu, B. Liu, Q. Wang, Y. Gao, Y. Shi, X. Feng, X. An, L. Liu, J. Zhang, Ionic liquid assisted chemical strategy to TiO2 hollow nanocube assemblies with surface-fluorination and nitridation and high energy crystal facet exposure for enhanced photocatalysis, ACS Appl. Mater. Interfaces 6 (2014) 10283–10295.
[14] R. Ramanathan, V. Bansal, Ionic liquid mediated synthesis of nitrogen, carbon and fluorine-codoped rutile TiO2 nanorods for improved UV and visible light photocatalysis, RSC Adv. 5 (2015) 1424–1429.
[15] K. Yoo, H. Choi, D. Dionysiou, Ionic liquid assisted preparation of nanostructured TiO2 particles, Chem. Commun. (2004) 2000–2001.
[16] S. Chang, C. Lee, A salt-assisted approach for the pore-size-tailoring of the ionic-liquid-templatedTiO2 photocatalysts exhibiting high activity, Appl. Catal. B: Environ. 132–133 (2013) 219–228.
[17] M. Paszkiewicz, J. Łuczak, W. Lisowski, P. Patyk, A. Zaleska-Medynska, The ILs-assisted solvothermal synthesis of TiO2 spheres: the effect of ionic liquids on morphology and photoactivity of TiO2, Appl. Catal. B: Environ. 184 (2016) 223–237.
[18] H. Kaper, M.-G. Willinger, I. Djerdj, S. Gross, M. Antonietti, B.M. Smarsly, IL-assisted synthesis of V2O5 nanocomposites and VO2 nanosheets, J. Mater. Chem. 18 (2008) 5761–5769.
[19] A. Serrà, E. Gómez, J.F. López-Barbera, J. Nogués, E. Vallés, Green electrochemical template synthesis of CoPt nanoparticles with tunable size, composition, and magnetism from microemulsions using an ionic liquid (bmimPF6), ACS Nano 8 (2014) 4630–4639.
[20] E.E. Zvereva, S. Grimme, S.A. Katsyuba, V.V. Ermolaev, D.A. Arkhipova, N. Yan, V.A. Miluykov, O.G. Sinyashin, A. Aleksandrov, Solvation and stabilization of palladium nanoparticles in phosphonium-based ionic liquids: a combined infrared spectroscopic and density functional theory study, Phys. Chem. Chem. Phys. 16 (2014) 20672–20680.

[21] J. Piekart, J. Łuczak, Transport properties of microemulsions with ionic liquid apolar domains as a function of ionic liquid content, RSC Adv. 6 (2016) 92605–92620.
[22] IUPAC, Ionic Liquids Database, Ionic Liquids Database, Physical and Biophysical Chemistry Division, 2003.
[23] J.M. Macak, P. Schmuki, Anodic growth of self-organized anodic TiO2 nanotubes in viscous electrolytes, Electrochim. Acta 52 (2006) 1258–1264.
[24] A. Zielińska-Jurek, M. Walicka, A. Tadajewska, I. Łącka, M. Gazda, A. Zaleska, Preparation of Ag/Cudoped titanium (IV) oxide nanoparticles in w/o microemulsion, Physicochem. Probl. Miner. Process. 45 (2010) 113–126.
[25] A. Zielińska-Jurek, E. Kowalska, J.W. Sobczak, W. Lisowski, B. Ohtani, A. Zaleska, Preparation and characterization of monometallic (Au) and bimetallic (Ag/Au) modified-titania photocatalysts activated by visible light, Appl. Catal. B: Environ. 101 (2011) 504–514.
[26] S.E. John, S.K. Mohapatra, M. Misra, Double-wall anodic titania nanotube arrays for water photooxidation, Langmuir 25 (2009) 8240–8247.
[27] H. Wender, A.F. Feil, L.B. Diaz, C.S. Ribeiro, G.J. Machado, P. Migowski, D.E. Weibel, J. Dupont, S.R. Teixeira, Self-organized TiO2 nanotube arrays: synthesis by anodization in an ionic liquid and assessment of photocatalytic properties, ACS Appl. Mater. Interfaces 3 (2011) 1359–1365.
[28] J. Rodríguez-Carvajal, Recent advances in magnetic structure determination by neutron powder diffraction, Physica B 192 (1993) 55–69.
[29] M. Nischk, P. Mazierski, M. Gazda, A. Zaleska, Ordered TiO2 nanotubes: the effect of preparation parameters on the photocatalytic activity in air purification process, Appl. Catal. B: Environ. 144 (2014) 674–685.
[30] M. Długokęcka, J. Łuczak, Ż. Polkowska, A. Zaleska-Medynska, The effect of microemulsion composition on the morphology of Pd nanoparticles deposited at the surface of TiO2 and photoactivity of Pd-TiO2, Appl. Surf. Sci. 405 (2017) 220–230.
[31] M. Klein, J. Nadolna, A. Gołąbiewska, P. Mazierski, T. Klimczuk, H. Remita, A. Zaleska-Medynska, The effect of metal cluster deposition route on structure and photocatalytic activity of mono- and bimetallic nanoparticles supported on TiO2 by radiolytic method, Appl. Surf. Sci. 378 (2016) 37–48.
[32] J.M. Macak, H. Tsuchiya, L. Taveira, S. Aldabergerova, P. Schmuki, Smooth anodic TiO2 nanotubes, Angew. Chem. Int. Ed. 44 (2005) 7463–7465.
[33] H. Tokuda, K. Hayamizu, K. Ishii, Abu Bin Hasan Susan, M. Watanabe, Physicochemical properties and structures of room temperature ionic liquids. 2. Variation of alkyl chain length in imidazolium cation, J. Phys. Chem. B 109 (2005) 6103–6110.
[34] K.N. Marsh, J.A. Boxall, R. Lichtenthaler, Room temperature ionic liquids and their mixtures—a review, Fluid Phase Equilib. 219 (2004) 93–98.
[35] N.G. Tsierkezos, I. Molinou, Thermodynamic properties of water + ethylene glycol at 283.15, 293.15, 303.15, and 313.15 K, J. Chem. Eng. Data 43 (1998) 989–993.
[36] A. Valota, D.J. LeClere, P. Skeldon, M. Curioni, S.B.T. Hashimoto, J. Kunze, P. Schmuki, G.E. Thompson, Influence of water content on nanotubular anodic titania formed in fluoride/glycerol electrolytes, Electrochim. Acta 54 (2009) 4321–4327.
[37] A. Elsanousi, J. Zhang, H.M.H. Fadlalla, Feng Zhang, Hui Wang, Xiaoxia Ding, Zhixin Huang, Chengcun Tang, Self-organized TiO2 nanotubes with controlled dimensions by anodic oxidation, J. Mater. Sci. 43 (2008) 7219–7224.
[38] W. Zhao, W. Ma, C. Chen, J. Zhao, Z. Shuai, Efficient degradation of toxic organic pollutants with ni2O3/TiO2-xBx under visible irradiation, J. Am. Chem. Soc. 126 (2004) 4782–4783.
[39] X. Pan, M.-Q. Yang, X. Fu, N. Zhang, Y.-J. Xu, Defective TiO2 with oxygen vacancies: synthesis, properties and photocatalytic applications, Nanoscale 5 (2013) 3601–3614.
[40] G. Xue, Q. Dai, S. Jiang, Chemical reactions of imidazole with metallic silver studied by the use of SERS and XPS techniques, J. Am. Chem. Soc. 110 (1988) 2393–2395.
[41] G. Bhargava, R.A. Ramanarayanan, S.L. Bernasek, Imidazole-Fe interaction in an aqueous chloride medium: effect of cathodic reduction of the native oxide, Langmuir 26 (2010) 215–219.
[42] Y. Wang, G.A. Voth, Tail aggregation and domain diffusion in ionic liquids, J. Phys. Chem. B 110 (2006) 18601–18608.
[43] K.-S. Kim, D. Demberelnyamba, H. Lee, Size-selective synthesis of gold and platinum nanoparticles using novel thiol-Functionalized ionic liquids, Langmuir 20 (2003) 556–560.
[44] B. Derjaguin, L. Landau, Theory of the stability of strongly charged lyophobic sols and of the adhesion of strongly charged particles in solutions of electrolytes, Prog. Surf. Sci. 43 (1993) 30–59.
[45] M. Olschewski, R. Gustus, M. Marschewski, O. Höfft, F. Endres, Spectroscopic characterization of the interaction of lithium with thin films of the ionic liquid 1-octyl-3-methylimidazolium bis(trifluoromethylsulfonyl)amide, Phys. Chem. Chem. Phys. 16 (2014) 25969–25977.
[46] H. Li, J. Xing, Z. Xia, J. Chen, Preparation of extremely smooth and boron-fluorine co-doped TiO2 nanotube arrays with enhanced photoelectrochemical and photocatalytic performance, Electrochim. Acta 139 (2014) 331–336.
[47] K. Anderson, S. Cortiñas Fernández, C. Hardacre, P.C. Marr, Preparation of nanoparticulate metal catalysts in porous supports using an ionic liquid route; hydrogenation and CC coupling, Inorg. Chem. Commun. 7 (2004) 73–76.
[48] M.G. Freire, C.M.S.S. Neves, I.M. Marrucho, J.A.P. Coutinho, M. Fernandes, Hydrolysis of tetrafluoroborate and hexafluorophosphate counter ions inImidazolium-based ionic liquids, J. Phys. Chem. A 114 (2010) 3744–3749.
[49] C.A. Wamser, Hydrolysis of fluoboric acid in aqueous solution, J. Am. Chem. Soc. 70 (1947) 1209–1215.
[50] N.R. Jana, L. Gearheart, C.J. Murphy, Seed-mediated growth approach for shape-controlled synthesis of spheroidal and rod-like gold nanoparticles using a surfactant template, Adv. Mater. 13 (2001) 1389–1393.
[51] A. Subramanian, H.-W. Wang, Effects of boron doping in TiO2 nanotubes and the performance of dye-sensitized solar cells, Appl. Surf. Sci. 258 (2012) 6479–6484.
[52] J.M. Macak, H. Tsuchiya, A. Ghicov, K. Yasuda, R. Hahn, S. Bauer, P. Schmuki, TiO2 nanotubes: self-organized electrochemical formation, properties and applications, Curr. Opin. Solid State Mater. Sci. 11 (2007) 3–18.
[53] K. Lee, J. Kim, H. Kim, Y. Lee, Y. Tak, D. Kim, P. Schmuki, Effect of electrolyte conductivity on the formation of a nanotubular TiO2 photoanode for a dye-sensitized solar cell, J. Korean Phys. Soc. 54 (2009) 1027–1031.
[54] C.D. Jaeger, A.J. Bard, Spin trapping and electron spin resonance detection of radical intermediates in the photodecomposition of water at TiOp particulate systems, J. Phys. Chem. 83 (1979) 3146–3152.
[55] C.S. Turchi, D.F. Ollis, Photocatalytic degradation of organic water contaminants: mechanisms involving hydroxyl radical photocatalytic degradation of organic water contaminants: mechanisms involving hydroxyl radical attack, J. Catal. 122 (1990) 178–192.
[56] Z. Liu, X. Zhang, S. Nishimoto, T. Murakami, A. Fujishima, Efficient photocatalytic degradation of gaseous acetaldehyde by highly ordered TiO2 nanotube arrays, Environ. Sci. Technol. 42 (2008) 8547–8551.
[57] A.G. Kontos, A. Katsanaki, T. Maggos, V. Likodimos, A. Ghicov, D. Kim, J. Kunze, C. Vasilakos, P. Schmuki, P. Falaras, Photocatalytic degradation of gas pollutants on self-assembled titania nanotubes, Chem. Phys. Lett. 490 (2010) 58–62.
[58] P. Mazierski, M. Nischk, M. Gołkowska, W. Lisowski, M. Gazda, M.J. Winiarski, T. Klimczuk, A. Zaleska-Medynska, Photocatalytic activity of nitrogen doped TiO2 nanotubes prepared by anodic oxidation: the effect of applied voltage, anodization time and amount of nitrogen dopant, Appl. Catal. B: Environ. 196 (2016) 77–88.
[59] S.-J. Hsu, I.J.B. Lin, Synthesis of gold nanosheets through thermolysis of mixtures of long chain 1-alkylimidazole and hydrogen tetrachloroaurate(III), J. Chin. Chem. Soc. 56 (2009) 98–106.
[60] H.-F. Zhuang, C.-J. Lin, Y.-K. Lai, L. Sun, J. Li, Some critical structure factors of titanium oxide nanotube array in its photocatalytic activity, Environ. Sci. Technol. 41 (2007) 4735–4740.
[61] L.G. Devi, R. Kavitha, A review on non metal ion doped titania for the photocatalytic degradation of organic pollutants under UV/solar light: role of photogenerated charge carrier dynamics in enhancing the activity, Appl. Catal. B: Environ. 140–141 (2013) 559–587.
[62] R. Asahi, T. Morikawa, H. Irie, T. Ohwaki, Nitrogen-doped titanium dioxide as visible-light-sensitive photocatalyst: designs, developments, and prospects, Chem. Rev. 114 (2014) 9824–9852.
[63] X. Chen, L. Liu, F. Huang, Black titanium dioxide (TiO2) nanomaterials, Chem. Soc. Rev. 44 (2015) 1861–1885.
[64] K.M. Manamela, L.C. Murulana, M.M. Kabanda, E.E. Ebenso, Adsorptive and DFT studies of some imidazolium based ionic liquids as corrosion inhibitors for zinc in acidic medium, Int. J. Electrochem. Sci. 9 (2014) 3029–3046.
[65] H.-C. Liang, X.-Z. Li, Effects of structure of anodic TiO2 nanotube arrays on photocatalytic activity for the degradation of 2,3-dichlorophenol in aqueous solution, J. Hazard. Mater. 162 (2009) 1415–1422.
[66] X. Li, P. Liu, Y. Mao, M. Xing, J. Zhang, Preparation of homogeneous nitrogen-doped mesoporous TiO2 spheres with enhanced visible-light photocatalysis, Appl. Catal. B: Environ. 164 (2015) 352–359.
[67] D. Nassoko, Y.-F. Li, H. Wang, J.-L. Li, Y.-Z. Li, Y. Yu, Nitrogen-doped TiO2 nanoparticles by using EDTA as nitrogen source and soft template: simple preparation, mesoporous structure, and photocatalytic activity under visible light, J. Alloys Compd. 540 (2012) 228–235.
[68] P. Mazierski, W. Lisowski, T. Grzyb, M.J. Winiarski, T. Klimczuk, A. Mikołajczyk, J. Flisikowski, A. Hirsch, A. Kołakowska, T. Puzyn, A. Zaleska-Medynska, J. Nadolna, Enhanced photocatalytic properties of lanthanide-TiO2 nanotubes: an experimental and theoretical study, Appl. Catal. B: Environ. 205 (2017) 376–385.
[69] E. Grabowska, J. Reszczyńska, A. Zaleska, Mechanism of phenol photodegradation in the presence of pure and modified-TiO2: a review, Water Res. 46 (2012) 5453–5471.
[70] B. Tryba, A.W. Morawski, M. Inagaki, M. Toyoda, The kinetics of phenol decomposition under UV irradiation with and without H2O2 on TiO2, FeeTiO2 and FeeCeTiO2 photocatalysts, Appl. Catal. B: Environ. 63 (2006) 215–221.
[71] B. Tryba, A.W. Morawski, M. Inagaki, M. Toyoda, Mechanism of phenol decomposition on Fe-C-TiO2 and Fe TiO2 photocatalysts via photo-Fenton process, J. Photochem. Photobiol. A: Chem. 179 (2006) 224–228.